AIAA-91-0388

Magnetohydrodynamic Flow Computations in Three Dimensions

S. Lee and G. Dulikravich
The Pennsylvania State University
University Park, PA

29th Aerospace Sciences Meeting
January 7–10, 1991/Reno, Nevada

MAGNETOHYDRODYNAMIC FLOW COMPUTATIONS IN THREE DIMENSIONS

Seungsoo Lee* and George S. Dulikravich**
Department of Aerospace Engineering
Penn State University, University Park, PA. 16802
USA

Abstract

A complete three-dimensional mathematical model has been developed governing steady, laminar flow of an incompressible fluid subjected to a magnetic field and including internal heating due to Joule effect, heat transfer due to conduction, and thermally induced buoyancy forces. The thermally induced buoyancy was accounted for via Boussinesque approximation. The entire system of eight partial differential equations was solved by integrating intermittently a system of five fluid flow equations and a system of three magnetic field equations and transferring the information through source-like terms. Explicit Runge-Kutta time-stepping algorithm and finite difference scheme with artificial compressibility were used in the general non-orthogonal curvilinear boundary conforming coordinate system. Comparison of computational results and known analytical solutions in two and three dimensions demonstrates high accuracy and smooth monotone convergence of the iterative algorithm. Results of test cases with thermally induced buoyancy demonstrate the stabilizing effect of the magnetic field on the recirculating flows.

Introduction

It is a well-known fact that magnetic field has a strong effect on fluid flows. For example, a Poiseuille velocity profile flattens due to the applied magnetic field. In the presence of the magnetic field, the strengths of vortices produced by thermal instability can be reduced. Engineers have used the properties of the magnetic field in applications ranging from flowmeters to space processing.

Despite its importance in engineering applications, only few attempts [1,2] have been made to simulate magnetohydrodynamic phenomena numerically. However, these works were restricted to two-dimensional problems. In the present paper, a complete three-dimensional numerical simulation of steady, laminar, magnetohydrodynamic incompressible flow was performed, although the numerical procedure can be extended to compressible flows. The first part of this paper presents a mathematical model of magneto-hydrodynamics. The electric field vector is eliminated from the Maxwell's equations using Joule's law. This results in magnetic transport equations, which consist of three partial differential equations of mixed hyperbolic-parabolic type. These magnetic transport equations are integrated along with Navier-Stokes equations. The second part of the paper presents the numerical method for solving the system of the governing equations. The system of equations is split into two systems of equations: the system for the fluid flow field and the system for the magnetic field. Such a splitting approach was used by a number of researchers to solve the Navier-Stokes equations with k-ε equations of turbulence [3,4]. One of the advantages of this approach is that the additional equations (turbulence, magnetic field, etc.) can be included without modifying existing basic flow solver. On the other hand, slightly adverse effect on numerical stability could be expected as the result of partially "decoupling" the global system.

* Postdoctoral Fellow. Member AIAA. Presently with Korean Defence Agency, Daejon, S. Korea.
** Associate Professor. Senior Member AIAA

A stability analysis of this approach was performed in conjunction with an explicit Runge-Kutta method.The stability analysis was performed by considering an equivalent multi-stage scheme similar to the split Runge-Kutta procedure. Stability results show that the split procedure does not change the stability of the global scheme significantly. As long as the CFL condition for each individual system is separately satisfied, the stability condition for the split approach is satisfied.

Governing Equations

After ignoring the electric displacement vector, Maxwell's equations [5] can be written in Cartesian tensor notation as

$$H_{i,i} = 0 \tag{1}$$

$$\varepsilon_{ijk} H_{k,j} = \frac{4\pi}{c} J_i \tag{2}$$

$$\varepsilon_{ijk} E_{k,j} = -\frac{\mu}{c} H_{i,t} \tag{3}$$

where ε_{ijk} is the permutation symbol, and commas designate differentiation. Here, H_i, and E_i are the components of the magnetic field vector and the electric field vector, while c, μ, and t are the speed of light, the magnetic permeability, and the time, respectively. The equations are cast in Gaussian units and the repeated index denotes the summation over the index. Joule's law is given by

$$J_i = \sigma\left(E_i + \frac{\mu}{c}\varepsilon_{ijk} v_j H_k\right) \tag{4}$$

where J_i, and v_i are the components of the current density vector, and the fluid velocity vector, respectively. Coefficient σ is the electrical conductivity.

With the aid of the Boussinesque approximation [6], Navier-Stokes equations for the incompressible electrically conducting homo-compositional fluid flow including buoyancy force are given by mass conservation:

$$v_{i,i} = 0 \tag{5}$$

momentum conservation:

$$v_{i,t} + (v_i v_j)_{,j} = -\frac{1}{\rho} p_{,i} + \frac{\eta}{\rho} v_{i,jj} + \frac{\mu}{c\rho} \varepsilon_{ijk} J_j H_k - \alpha g_i (T - T_c) \tag{6}$$

and energy conservation:

$$T_{,t} + (v_j T)_{,j} = \kappa T_{,jj} + \frac{J_j J_j}{\rho \sigma c_p} \tag{7}$$

where g_i, ρ, p, and T are the gravity components, the fluid density, the sum of hydrodynamic pressure and the hydrostatic pressure, and the temperature, respectively. Here, η, α, κ and c_p are the coefficients of viscosity, thermal expansion, thermal diffusivity, and specific heat, respectively. The third term on the right hand side of the momentum equation is the Lorentz force due to the magnetic filed. The last term on the right hand side of the momentum equation is the thermal buoyancy force. Notice that the viscous dissipation terms are neglected, while the Joule heating is included in the energy equation in accordance with the Boussinesque approximation.

Eliminating E_i between the Maxwell's equations, Eqs. (1), (2) and (3), we have the so-called magnetic transport equations.

$$H_{i,t} + (v_j H_i - v_i H_j)_{,j} = \frac{c^2}{4\pi\mu\sigma} H_{i,jj} \tag{8}$$

From the definition of the current density vector, Eq. (4), and the vector identities, the momentum equations, Eq. (6), can be written as

$$v_{i,t} + \left(v_i v_j - \frac{\mu}{4\pi} H_i H_j\right)_{,j} = -\frac{1}{\rho} p^*_{,i} + \frac{\eta}{\rho} v_{i,jj} - \alpha g_i (T - T_c) \tag{9}$$

where the combination of the hydrostatic, hydrodynamic, and magnetic field pressure is

$$p^* = p + \frac{\mu H_i H_i}{8\pi} \tag{10}$$

For convenience, the superscript * will be dropped.

Non-Dimensionalization

It is desirable to non-dimensionalize the governing equations in order to simplify the study of the relative importance of each physical phenomenon involved. The following non-dimensional form of the governing equations is obtained

$$v_{i,i} = 0 \tag{11}$$

$$v_{i,t} + \left(v_i v_j - \frac{Ht}{RmRe} H_i H_j\right)_{,j} = - p_{,i} + \frac{1}{Re} v_{i,jj} - \frac{Gr}{Re^2} e_i \theta \tag{12}$$

$$\theta_{,t} + (v_j\theta)_{,j} = \frac{1}{PrRe} \theta_{,jj} + \varepsilon_m \tag{13}$$

and

$$H_{i,t} + (v_j H_i - v_i H_j)_{,j} = \frac{1}{Rm} H_{i,jj} \tag{14}$$

Here, θ is the normalized temperature, $\frac{T - T_c}{\Delta T}$, and $\Delta T = T_h - T_c$, where T_h and T_c are two reference temperatures. The unit vector in the direction of gravitational vector is designated as e_i. The term due to Joule heating becomes

$$\varepsilon_m = \frac{EcHt^2}{RmRe^2} \varepsilon_{ijk}\varepsilon_{ilm} H_{k,j} H_{m,l} \tag{15}$$

and the non-dimensional numbers are given by

Eckert number $\quad Ec = \dfrac{v_r^2}{c_p \Delta T}$

Grashof number $\quad Gr = \dfrac{\rho \alpha g l_r^3 \Delta T}{\eta^2}$

Hartman number $\quad Ht = \mu l_r H_r \sqrt{\dfrac{\sigma}{c^2 \eta}}$

Magnetic Reynolds number $\quad Rm = RePm = \dfrac{4\pi\mu\sigma v_r l_r}{c^2}$

Hydrodynamic Reynolds number $\quad Re = \dfrac{\rho v_r l_r}{\eta}$

Magnetic Prandtl number $\quad Pm = \dfrac{4\pi\mu\sigma\eta}{\rho c^2}$

Prandtl number $\quad Pr = \dfrac{\eta c_p}{\kappa}$

Numerical Algorithm

The equations (11), (12), (13) and (14) represent a global system of highly coupled non-linear partial differential equations. For simplicity of computer programming the system is split into two systems. Equations (11), (12) and (13) constitute the first system, and Eqs. (14) constitute the second system. Each system is integrated by the explicit Runge-Kutta time stepping method [7] in an alternating manner.

After transformation to generalized curvilinear non-orthogonal coordinates, the systems of governing equations can be written in fully conservative form as

$$\frac{\partial Q}{\partial t} + \frac{\partial E}{\partial \xi} + \frac{\partial F}{\partial \eta} + \frac{\partial G}{\partial \zeta} = D^2 + D \tag{16}$$

For the flow field part of the global system, the solution vector Q, the flux vectors E, F, G and the source vector D are given by

$$Q = \frac{1}{J}\begin{bmatrix} 0 \\ u \\ v \\ w \\ \theta \end{bmatrix} \quad E = \frac{1}{J}\begin{bmatrix} U \\ Uu + \xi_x p \\ Uv + \xi_y p \\ Uw + \xi_z p \\ U\theta \end{bmatrix} \quad F = \frac{1}{J}\begin{bmatrix} V \\ Vu + \eta_x p \\ Vv + \eta_y p \\ Vw + \eta_z p \\ V\theta \end{bmatrix}$$

$$G = \frac{1}{J}\begin{bmatrix} W \\ Wu + \zeta_x p \\ Wv + \zeta_y p \\ Ww + \zeta_z p \\ W\theta \end{bmatrix} \quad D = \begin{bmatrix} 0 \\ d_2 \\ d_3 \\ d_4 \\ d_5 \end{bmatrix} \tag{17}$$

where $J = \dfrac{\partial(\xi,\eta,\zeta)}{\partial(x,y,z)}$ is the Jacobian determinant of the geometric transformation from x, y, z into ξ, η, ζ computational space.

Here,

$$d_2 = \frac{Ht^2}{RmRe}\left[\frac{\partial}{\partial\xi}\left\{\frac{\hat{H}_\xi H_1}{J}\right\} + \frac{\partial}{\partial\eta}\left\{\frac{\hat{H}_\eta H_1}{J}\right\} + \frac{\partial}{\partial\zeta}\left\{\frac{\hat{H}_\zeta H_1}{J}\right\}\right]$$

$$- \frac{Gr\theta}{Re^2 J} e_\xi$$

$$d_3 = \frac{Ht^2}{RmRe}\left[\frac{\partial}{\partial\xi}\left\{\frac{\hat{H}_\xi H_2}{J}\right\} + \frac{\partial}{\partial\eta}\left\{\frac{\hat{H}_\eta H_2}{J}\right\} + \frac{\partial}{\partial\zeta}\left\{\frac{\hat{H}_\zeta H_2}{J}\right\}\right]$$

$$- \frac{Gr\theta}{Re^2 J} e_\eta$$

$$d_4 = \frac{Ht^2}{RmRe}\left[\frac{\partial}{\partial\xi}\left\{\frac{\hat{H}_\xi H_3}{J}\right\} + \frac{\partial}{\partial\eta}\left\{\frac{\hat{H}_\eta H_3}{J}\right\} + \frac{\partial}{\partial\zeta}\left\{\frac{\hat{H}_\zeta H_3}{J}\right\}\right]$$

$$- \frac{Gr\theta}{Re^2 J} e_\zeta$$

$$d_5 = \frac{EcHt^2 J}{RmRe^2}\left[A_1^2 + A_2^2 + A_3^2\right] \qquad (18)$$

where H_1, H_2, H_3 are the components of the magnetic field vector in Cartesian coordinates, and

$$A_1 = \frac{\partial}{\partial\xi}\left[\frac{H_3\xi_y - H_2\xi_z}{J}\right] + \frac{\partial}{\partial\eta}\left[\frac{H_3\eta_y - H_2\eta_z}{J}\right]$$

$$+ \frac{\partial}{\partial\zeta}\left[\frac{H_3\zeta_y - H_2\zeta_z}{J}\right]$$

$$A_2 = \frac{\partial}{\partial\xi}\left[\frac{H_1\xi_z - H_3\xi_x}{J}\right] + \frac{\partial}{\partial\eta}\left[\frac{H_1\eta_z - H_3\eta_x}{J}\right]$$

$$+ \frac{\partial}{\partial\zeta}\left[\frac{H_1\zeta_z - H_3\zeta_x}{J}\right]$$

$$A_3 = \frac{\partial}{\partial\xi}\left[\frac{H_2\xi_x - H_1\xi_y}{J}\right] + \frac{\partial}{\partial\eta}\left[\frac{H_2\eta_x - H_1\eta_y}{J}\right]$$

$$+ \frac{\partial}{\partial\zeta}\left[\frac{H_2\zeta_x - H_1\zeta_y}{J}\right] \qquad (19)$$

The physical viscous dissipation term is transformed to

$$D^2 = \left[\frac{S}{J} g_{ij}(JQ)_{,j}\right]_{,i} \qquad (20)$$

where

$$g_{ij} = \nabla x'_i \nabla x'_j \qquad (21)$$

$$S = \mathrm{diag}\left[0, \frac{1}{Re}, \frac{1}{Re}, \frac{1}{Re}, \frac{1}{PrRe}\right] \qquad (22)$$

The contravariant components U, V, W of the velocity vector are related to the velocity components u, v, w in the Cartesian system as follows

$$\begin{bmatrix} U \\ V \\ W \end{bmatrix} = \begin{bmatrix} \xi_x & \xi_y & \xi_z \\ \eta_x & \eta_y & \eta_z \\ \zeta_x & \zeta_y & \zeta_z \end{bmatrix} \begin{bmatrix} u \\ v \\ w \end{bmatrix} \qquad (23)$$

Similarly, the contravariant components $\hat{H}_\xi$, $\hat{H}_\eta$, $\hat{H}_\zeta$ of the magnetic field vector are defined as

$$\begin{bmatrix} \hat{H}_\xi \\ \hat{H}_\eta \\ \hat{H}_\zeta \end{bmatrix} = \begin{bmatrix} \xi_x & \xi_y & \xi_z \\ \eta_x & \eta_y & \eta_z \\ \zeta_x & \zeta_y & \zeta_z \end{bmatrix} \begin{bmatrix} H_1 \\ H_2 \\ H_3 \end{bmatrix} \qquad (24)$$

In order to integrate the system simultaneously and obtain a time-asymptotic solution, an artificial compressibility [8] term , $\frac{\partial}{\partial t}\left(\frac{p}{\beta J}\right)$, is added to the solution vector resulting in

$$Q = \frac{1}{J}\begin{bmatrix} p/b \\ u \\ v \\ w \\ \theta \end{bmatrix} \qquad (25)$$

For the system of magnetic field equations, the solution vector Q, the flux vectors E, F, G, and the source vector D are given by

$$Q = \frac{1}{J}\begin{bmatrix} H_1 \\ H_2 \\ H_3 \end{bmatrix} \quad E = \frac{1}{J}\begin{bmatrix} H_1U - u\hat{H}_\xi \\ H_2U - v\hat{H}_\xi \\ H_3U - w\hat{H}_\xi \end{bmatrix} \quad F = \frac{1}{J}\begin{bmatrix} H_1V - u\hat{H}_\eta \\ H_2V - v\hat{H}_\eta \\ H_3V - w\hat{H}_\eta \end{bmatrix}$$

$$G = \frac{1}{J}\begin{bmatrix} H_1 W - u\hat{H}_\zeta \\ H_2 W - v\hat{H}_\zeta \\ H_3 W - w\hat{H}_\zeta \end{bmatrix} \qquad D = 0 \qquad S = \frac{I}{Rm} \qquad (26)$$

where I is the identity matrix of rank 3.

The Runge-Kutta time stepping method [7] given by

$$\begin{aligned} Q^0 &= Q^t \\ \Delta Q^k &= -\alpha_k \Delta t R^{k-1} \qquad k = 1,2,...,K \\ Q^{t+1} &= Q^t + \Delta Q^K \end{aligned} \qquad (27)$$

was used in time-integration of both systems. Here the residual vector is defined as

$$R = \frac{\partial E}{\partial \xi} + \frac{\partial F}{\partial \eta} + \frac{\partial G}{\partial \zeta} - D^2 - D + \frac{\delta}{8J\Delta t}\left[\frac{\partial^4}{\partial \xi^4} + \frac{\partial^4}{\partial \eta^4} + \frac{\partial^4}{\partial \zeta^4}\right](JQ) \qquad (28)$$

The last term of the residual vector is the fourth order artificial dissipation [7] where δ is the user specified small parameter and Δt is the time step. For the four stage (K=4) Runge-Kutta method, α_k = 1/4, 1/3, 1/2 and 1, respectively.

Boundary conditions

The system of the flow field equations is characterized by its hyperbolic nature. Therefore, the boundary conditions have to be applied by considering the characteristic directions. The eigenvalues of the Jacobian matrix of the flux vector E are

$$L = \mathrm{diag}(U-a, U+a, U, U, U) \qquad (29)$$

where a is the equivalent speed of sound

$$a = \sqrt{U^2 + \beta\left\{\xi_x^2 + \xi_y^2 + \xi_z^2\right\}}. \qquad (30)$$

At the inlet boundary, one of the eigenvalues is negative. As a results, four boundary conditions should be imposed there. In this study, the incoming velocity components, u, v, w and the temperature, θ, are specified. The pressure, p, is computed from the characteristic equation. At the exit boundary, one boundary condition should be imposed. We specified the pressure, while the velocity components and the temperature were obtained by integrating the characteristic equations.

The application of the boundary conditions is given as follows [10,11]. Premultiplying the equations by the similarity transformation matrix, M_ξ^{-1} (in ξ direction), Eq. (27) results in the characteristic form of the equations. The equation corresponding to the negative eigenvalue is to be selected at the inlet, while at the exit the equations corresponding to positive eigenvalues are chosen. This selection procedure can be thought of as a matrix operation, and we designate the operator as L. If the boundary condition is given by Ω, then

$$\Omega^{t+1} = \Omega^t + \frac{\partial \Omega}{\partial Q}\Delta Q \qquad (31)$$

$$\text{or} \qquad \frac{\partial \Omega}{\partial Q}\Delta Q = -\Omega^t \qquad (32)$$

and the equation (32) is added to the transformed-selected equations, that is,

$$\left[LM_\xi^{-1} + \frac{\partial \Omega}{\partial Q}\right]\Delta Q = -\alpha_k \Delta t\left[M_\xi^{-1} R^{k-1} + \frac{\Omega^t}{\alpha_k \Delta t}\right] \qquad (33)$$

At the inlet plane,

$$L = \mathrm{diag}[1,0,0,0,0] \qquad (34)$$

$$\Omega = [\,0,\ u-u_p,\ v-v_p,\ w-w_p,\ \theta-\theta_p]^T \qquad (35)$$

At the exit plane,

$$L = \mathrm{diag}[0,1,1,1,1] \qquad (36)$$

$$\Omega = [p-p_p, 0, 0, 0, 0]^T \qquad (37)$$

so that $\frac{\partial \Omega}{\partial Q} = \mathrm{diag}[\beta J, 0, 0, 0, 0]$. The subscript p denotes the prescribed value and the superscript T designates the transpose of a vector. Along a solid wall, the velocity components were set to zero. The pressure was extrapolated from the interior point, while the temperature was either specified or extrapolated depending on the boundary condition type (Neumann or Dirichlet boundary condition).

The system of the magnetic field equations is also of hyperbolic type in time. The eigenvalues of

the Jacobian matrix of this system are L=diag[U,U,0] in case of ξ direction. At the inlet plane, therefore, two components of the magnetic field vector are specified, while the axial component H_1 of the magnetic field vector is evaluated from the characteristic equation. The transformation matrix for the magnetic transport equations is given by

$$M_\xi^{-1}=\begin{bmatrix} k_{23}v-k_{12}w & k_{31}w-k_{23}u & k_{12}u-k_{31}v \\ k_{23}w-k_{31}v & k_{31}u-k_{12}w & k_{12}v-k_{23}u \\ -\xi_x k_{123} & -\xi_y k_{123} & -\xi_z k_{123} \end{bmatrix} \tag{38}$$

where

$$k_{12} = \xi_3^2 - \xi_x\xi_y$$
$$k_{23} = \xi_1^2 - \xi_y\xi_z$$
$$k_{31} = \xi_2^2 - \xi_z\xi_x$$
$$k_{123} = k_{12} + k_{23} + k_{31} \tag{39}$$

and

$$L = \mathrm{diag}[1,1,0] \tag{40}$$

$$\Omega = [\, H_2-H_{2p},\, H_3-H_{3p},\, 0]^T \tag{41}$$

At the exit plane, all three variables are updated by integrating the governing equations.

Let $\langle\,\rangle$ denote the jump across the boundary. If the wall is a perfect conductor, the tangential component of the magnetic field experiences the discontinuity, but the normal component should be continuous

$$n \times \langle E \rangle = 0 \qquad n \cdot H = 0 \tag{42}$$

If the wall is a perfect insulator, the boundary condition takes a simpler form

$$\langle H \rangle = 0 \tag{43}$$

Stability Analysis

Consider a model system of equations

$$\frac{\partial Q}{\partial t} + A\frac{\partial Q}{\partial x} = 0 \tag{44}$$

where

$$Q = \begin{Bmatrix} u_1 \\ u_2 \end{Bmatrix} \qquad A = \begin{bmatrix} a_{11} & a_{12} \\ a_{21} & a_{22} \end{bmatrix} \tag{45}$$

The amplification matrix of the Runge-Kutta method for the unsplit approach can be found as

$$G = I - N + \frac{N^2}{2} - \frac{N^3}{6} + \frac{N^4}{24} \tag{46}$$

where

$$N = i\frac{\sin(\kappa\Delta x)}{\Delta x}\begin{bmatrix} a_{11} & a_{12} \\ a_{21} & a_{22} \end{bmatrix} \tag{47}$$

To be stable,

$$CFL = \frac{|\lambda|_{max}\Delta t}{\Delta x} \le 2\sqrt{2} \tag{48}$$

The Runge-Kutta method with the split approach can be thought of as a 2K stage multistage method, that is,

$$Q^k = Q^0 - \alpha_k\Delta t\begin{bmatrix} a_{11} & a_{12} \\ 0 & 0 \end{bmatrix}\frac{\partial Q^{k-1}}{\partial x} \quad \text{for } k=1,\cdots, K$$

$$Q^k = Q^K - \alpha_k\Delta t\begin{bmatrix} 0 & 0 \\ a_{21} & a_{22} \end{bmatrix}\frac{\partial Q^{k-1}}{\partial x} \quad \text{for } k=K+1,\cdots,2K;$$

with $$\alpha_{k+K} = \alpha_k \tag{49}$$

Define the provisional amplification matrix G_k for the first K stages as

$$Q^k = G_k Q^0 \tag{50}$$

Then we have the recursion formula for the provisional amplification matrix

$$G_k = I - \alpha_k\Delta t\tilde{N}_1 G_{k-1} \quad \text{for } k = 1,\cdots, K \tag{51}$$

where

$$G_0 = I \qquad \tilde{N}_1 = i\frac{\sin(\kappa\Delta x)}{\Delta x}\begin{bmatrix} a_{11} & a_{12} \\ 0 & 0 \end{bmatrix} \tag{52}$$

Similarly, define the provisional amplification matrix $\tilde{G}_k$ for the second K stages as

$$Q^k = \tilde{G}_k Q^K \tag{53}$$

we have

$$\tilde{G}_k = I - \alpha_k \Delta t \aleph_2 G_{k-1} \text{ for } k=K+1,\cdots,2K \quad (54)$$

where

$$\tilde{G}_K = I \qquad \aleph_2 = i\frac{\sin(\kappa\Delta x)}{\Delta x}\begin{bmatrix} 0 & 0 \\ a_{21} & a_{22} \end{bmatrix} \quad (55)$$

The amplification factor of the Runge-Kutta method for the split approach can be found as

$$G = G_K \tilde{G}_{2K} \quad (56)$$

If each amplification matrix satisfies the stability condition independently, that is, if

$$\rho(G_K) < 1 \qquad \rho(\tilde{G}_{2K}) < 1 \quad (57)$$

then there exists a consistent norm [13] such that

$$\|G_K\| < 1 \qquad \|\tilde{G}_{2K}\| < 1 \quad (58)$$

However from Eq. (55)

$$\rho(G_K \tilde{G}_{2K}) \le \|G_K \tilde{G}_{2K}\| \le \|G_K\| \, \|\tilde{G}_{2K}\| < 1 \quad (59)$$

where the first inequality is true for every norm, and the second inequality comes from the consistency of the norm. Thus, the split approach is stable. Notice that the actual stable region is broader than what is mentioned above. In general, if we split the system of equations into a number of systems, and if the stability conditions for each system are satisfied, then the complete system remains stable.

Computational Results

The first test case is the two-dimensional Hartman flow, which is equivalent to the Poiseuille flow in fluid dynamics. An H-type orthogonal grid of 50×20×20 cells was used in this computation (Fig. 1). The length of a duct was 15 times of the half height of the channel. The y-component of the magnetic field, H_0, on the solid walls was kept constant. As a result of the Lorentz force, the velocity profile is flatter than the velocity profile without the magnetic field. The hydrodynamic Reynolds number, Re based on the average velocity and the half of the channel height, was Re = 10 while the magnetic Reynolds number was Rm = 10. The Hartman number based on the imposed magnetic field and the half of the channel height was H_t = 5. The artificial compressibility coefficient of β = 10 was used.

In this computation, the influence of the buoyancy force was neglected. Therefore, the energy equation was decoupled from the rest of the equations. The imposed inlet velocity profile was that of Poiseuille flow. Since both Reynolds numbers are small, the flow develops fully over a short distance (Fig. 2). The pressure gradient becomes constant near the exit. Figure 3 compares the computed velocity profile with that of an analytical solution [5]. In Figure 4, the computed induced axial component of the magnetic field was compared with the analytic solution, showing excellent agreements. The relative error compared to the analytic solution is about 0.88 % for the axial velocity component, and 0.04 % for the axial component of the magnetic field. The convergence history of the test case is shown in Fig. 5. The code runs with 14 μ-sec per grid point per iteration on the Cray II computer.

The next test case is an equivalent Hartman flow in three dimensions. The computational domain was discretized with 50×20×20 rectangular clustered cells (Fig. 6). Both hydrodynamic and magnetic Reynolds numbers were 10. The value of the artificial compressibility coefficient was β = 10. Figure 7 shows the prescribed inlet velocity profile, which is fully developed laminar flow profile without magnetic field. The carpet plots of the analytic and computed x-component of velocity vector are shown in Fig. 8. The maximum relative error of the computed solution is 0.73 %. Figure 9 shows the analytic and computed x-component of the magnetic field. The computed solution deviates by less than 0.74 % from the analytic solution.

For completeness, the analytic solution [12] of the three-dimensional Hartman flow are given here.

$$\frac{u}{u_{av}} = \frac{4}{\pi^3}\left(\frac{b}{a}\right)^2 Re\,\hat{k} \times$$

$$\sum_{n=odd}^{\infty}\left[1 - \cosh\left\{\frac{H_t}{2}\left(\frac{y}{a} - 1\right)\right\}\sinh\left\{\frac{H_t\, y}{2a}\right\}\sinh^{-1}\left(\frac{H}{2}\right)\right.$$

$$\left. -\cosh\left(\frac{H_t\, y}{2a}\right)\sinh\left\{\frac{H_t}{2}\left(\frac{y}{a} - 1\right)\right\}\sinh^{-1}\left(\frac{H}{2}\right)\right] \frac{\sin\left(\frac{n\pi z}{b}\right)}{n^3}$$

The H_1 normalized with given H_2 component is

$$\frac{H_1}{H_2} = \frac{4}{\pi^3}\left(\frac{b}{a}\right)^2 \frac{Rm\,Re}{Ht}\hat{k} \times$$

$$\sum_{n=odd}^{\infty}\left[1 - \sinh\left\{\frac{Ht}{2}\left(\frac{y}{a} - 1\right)\right\}\sinh\left\{\frac{Ht\,y}{2a}\right\}\sinh^{-1}\left(\frac{H}{2}\right)\right.$$

$$\left.-\sinh\left(\frac{Ht\,y}{2a}\right)\sinh\left\{\frac{Ht}{2}\left(\frac{y}{a} - 1\right)\right\}\sinh^{-1}\left(\frac{H}{2}\right)\right]\frac{\sin\left(\frac{n\pi z}{b}\right)}{n^3} \tag{61}$$

Here, a and b are the width and the height of the channel, while

$$\frac{1}{Re} = 8\hat{k}\left(\frac{b}{a}\right)^2 \sum_{n=odd}^{\infty}\frac{1}{n^4}\left[1 + \left(\frac{b}{a}\right)^2\frac{H}{(n\pi)^2}\,\frac{\cosh\left(\frac{H}{2}\right) - \cosh\left(\frac{Ht}{2}\right)}{\sinh\left(\frac{H}{2}\right)}\right] \tag{62}$$

where the hydrodynamic and magnetic Reynolds numbers, Hartman number and the normalized pressure gradient are given by

$$Re = \frac{\rho u_{av}\,a}{\eta} \qquad \hat{k} = \frac{a}{\rho u_{av}^2}\frac{\partial p}{\partial x}$$

$$Ht = \mu a H_2\sqrt{\frac{\sigma}{c^2\eta}} \qquad Rm = \frac{4\pi\mu\sigma u_{av}a}{c^2} \tag{63}$$

Figure 10 shows the pressure, developing velocity profile, and the axial and vertical components of magnetic field vector normalized with the applied magnetic strength along the vertical mid-plane ($\frac{z}{a} = 0.5$). Both, flow field and magnetic field develop within two channel heights downstream from the inlet. The convergence history is plotted in Fig. 11. For this case the code executed at 15 μ-sec per grid point per iteration on Cray Y-MP computer.

The next example is the Bénard cell problem under the influence of magnetic field. The imposed magnetic field is parallel to the gravitation. To study the relative influence of the magnetic field, the computations were done both with and without the applied magnetic field. The Hartman number was 5, and the Grashof number was 3000 with the bottom wall hot, the top wall cold and the side walls thermally insulated. Since there is no reference velocity, the reference velocity was obtained by equating the magnitude of the buoyancy term to that of viscous term [14]. An orthogonal grid of 60×30 cells was used in this computation (Fig. 12). The artificial compressibility coefficient of $\beta = 1$ was used for both computations. Both the magnetic Prandtl number and the hydrodynamic Prandtl number were 1. Although no artificial dissipation was added, smooth solutions were obtained. The pressure along the solid wall was computed from the normal momentum equation [14].

Figure 13 shows isobar contours for computations with and without the applied magnetic field. As can be seen, the usual boundary condition for pressure, $\frac{\partial p}{\partial n}$, would have given erroneous results both with and without the influence of the magnetic field. The isothermal contours for both cases are plotted in Fig. 14. Figure 15 represents the streamlines for both cases. With the applied magnetic field, the strength of the vortices was weakened and the cells were elongated, which was predicted by Chandrasekhar [6] through a hydrodynamic linear stability analysis. Figure 16 depicts the lines of magnetic forces. They would be straight vertical lines without the flow induced by buoyancy. Figure 17 shows the convergence histories for both cases. It is noticeable that the convergence rate for the case with the applied magnetic field is much slower than without the magnetic field. It was found that with the Hartman number of 10 the circulatory motions from the thermal instability were damped significantly (Fig. 18). Though a thorough parametric study has not been performed, it is believed that the critical Hartman number beyond which the circulation would be entirely suppressed at Grashof number of 3000 is between 10 and 15.

Conclusions

Using the explicit approach, the governing equations of magnetohydrodynamics were solved with high accuracy. The stability analysis for a sample system shows that if each individual system satisfies the stability conditions, the complete system is stable. Numerical examples including the two- and three-dimensional Hartman flow were computed.

Recirculating flow generated by a thermally induced buoyancy was suppressed by the magnetic field.

Acknowledgements

The lead author would like to thank the Center for Cell Research at Penn State University for partially supporting this work. Computations were performed on the NAS facility at NASA Ames Research Center. Computing time was provided by Dr. Robert Stubbs of NASA Lewis Research Center. Graphics were produced on the equipment donated by Apple Computer Co., Inc.

References

1. Doss, E. D., Argyropoulos, G. S. and Demetriades, S. T., "Two-Dimensional Flow Inside MHD Ducts with Transverse Asymmetries," AIAA Journal, Vol. 13, May, 1975.
2. Feldman, L. A. and Burkhalter, J. E., "Numerical Solutions of Transient MHD Phenomena," AIAA Journal, Vol. 17, March, 1979.
3. Grasso, F., and Speziale, C. G., "Supersonic Flow Computations by Two-Equation Turbulence Modelling," AIAA Paper 89-1951 (1989).
4. Kunz, R. F., and Lakshminarayana, B., "Computation of Supersonic and Low Subsonic Cascade Flows Using an Explicit Navier-Stokes Technique and k-ε Turbulence Model", Proceedings of the CFD Symposium in Aeropropulsion, ed. M.-S. Liu, NASA Lewis Research Center, Cleveland, OH, April 24-26, 1990.
5. Jeffrey, A., Magnetohydrodynamics, University Mathematical Texts 33, Oliver & Royd LTD., Edinburgh, U.K, 1966.
6. Chandrasekhar, S., Hydrodynamic and Hydromagnetic Stability, Dover Publication Inc., New York, 1961.
7. Jameson, A., Schmidt, W., and Turkel, E., "Numerical Solutions of the Euler Equations by Finite Volume Methods Using Runge-Kutta Time-Stepping Scheme," AIAA paper 81-1259, Palo Alto, CA, June, 1981.
8. Chorin, A. J., "A Numerical Method for Solving Incompressible Viscous Flow Problems," Journal of Computational Physics, Vol. 2, 1967, pp. 12-26.
9. Steger, J. L. and Kutler, P., "Implicit Finite-Difference Procedure for the Computation of Vortex Wakes," AIAA Journal, Vol. 15, No. 7, July 1977, pp. 581-590.
10. Rogers, S. E., Kwak, D. and Chang, J. L. C., "INS3D-An Incompressible Navier-Stokes Code in Generalized Three-Dimensional Coordinates," NASA TM-100012, Nov. 1987.
11. Pan, D. and Chakravarthy, S., "Unified Formulation for Incompressible Flows," AIAA paper 89-0122, 27th Aerospace Sciences Meeting, Reno, Nevada, Jan. 9-12, 1989.
12. Sutton, G. W. and Sherman, A., Engineering Magnetohydrodynamics, McGraw-Hill Series in Mechanical Engineering, McGraw-Hill Book Company, 1965, pp 334-381.
13. Stewart, G. W., Introduction to Matrix Computations, Series in Computer Science and Applied Mathematics, Academic Press Inc., New York, 1973, pp. 284-289.
14. Lee, S., Acceleration of Iterative Algorithms for Euler and Navier-Stokes Equations, Ph.D. Thesis, The Department of Aerospace Engineering, The Pennsylvania State University, May 1990.

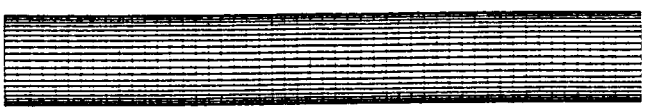

Figure 1. An H-type computational grid used for two-dimensional Hartman flow

(A) Isobar contours

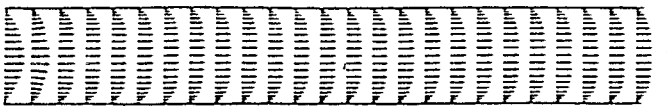

(B) Velocity vectors

(C) H_x/H_0

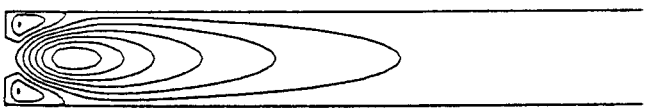

(D) H_y/H_0

Figure 2. Solutions of two-dimensional Hartman flow

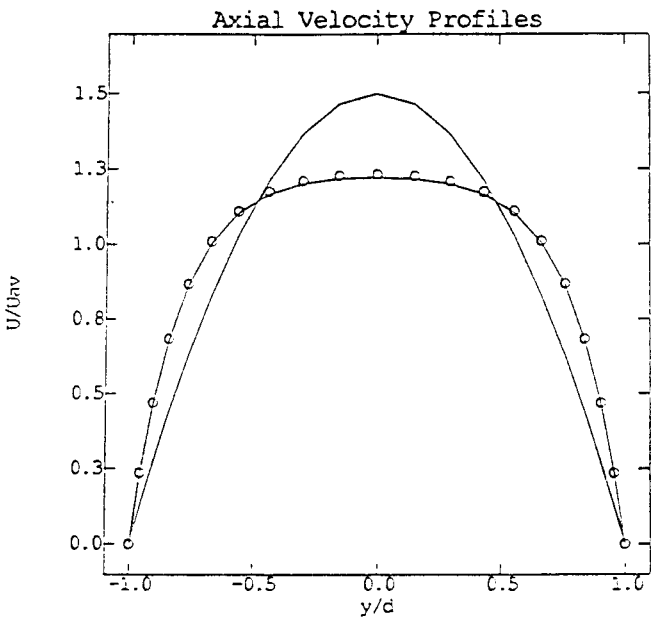

Figure 3. Axial velocity component at the exit (two-dimensional Hartman flow)
(- - - - inlet velocity; ------- computations; o o o o analytic solution)

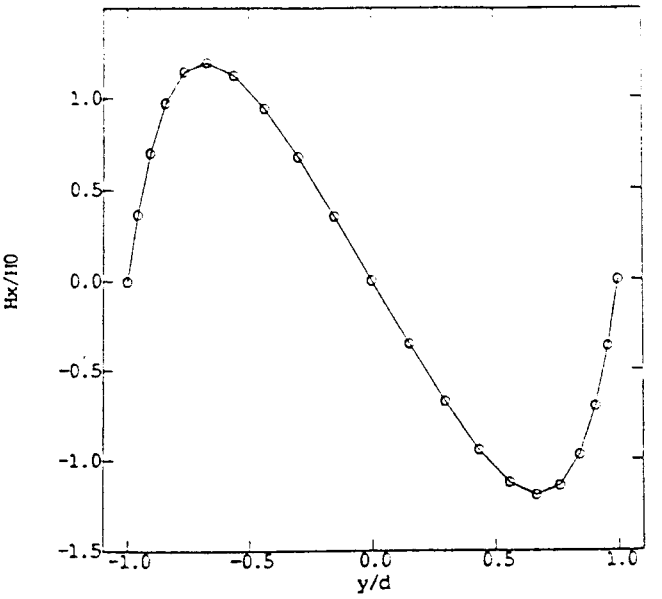

Figure 4. Axial magnetic field component at the exit (two-dimensional Hartman flow)
(------- computations; o o o o analytic solution)

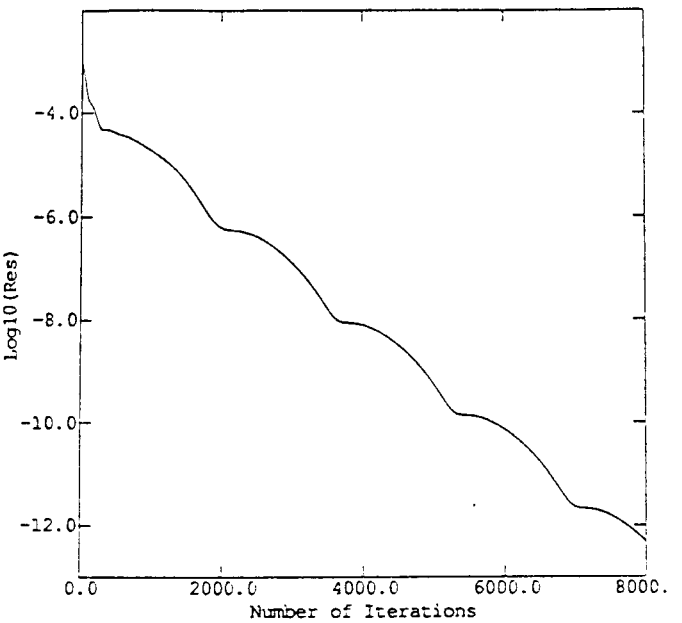

Figure 5. Convergence history (two-dimensional Hartman flow)

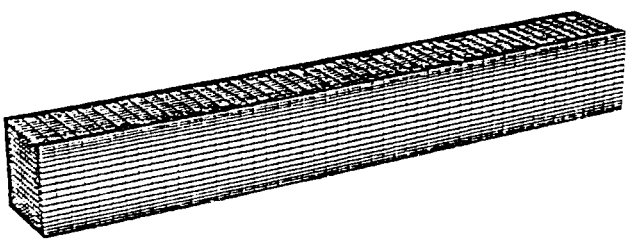

Figure 6. Computational domain for three-dimensional Hartman flow

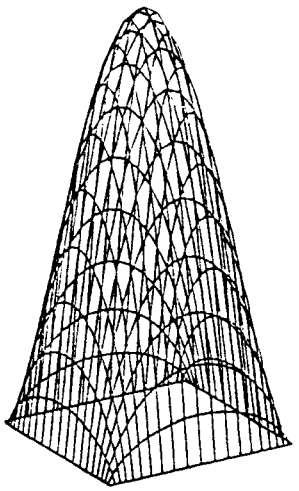

Figure 7. Inlet velocity profile

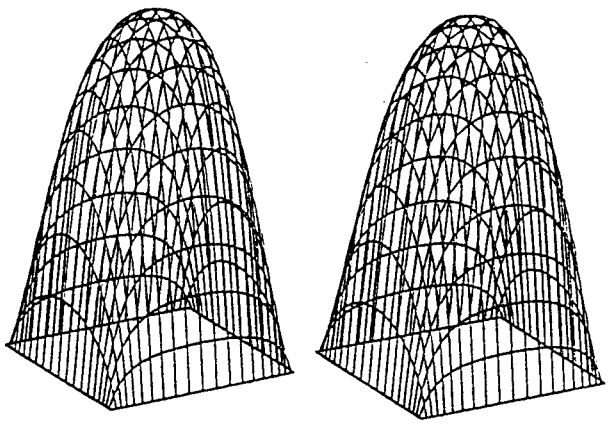

(A) Analytic solution (B) Computed solution

Figure 8. Axial component velocity profile

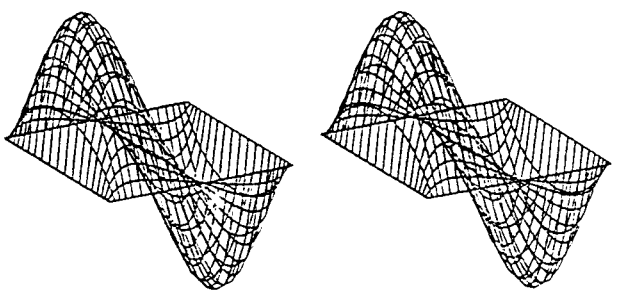

(A) Analytic solution (B) Computed solution

Figure 9. Axial component magnetic field vector

(A) Isobar contours

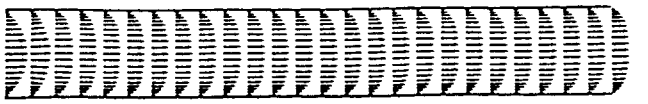

(B) Velocity vectors

(C) H_x/H_0

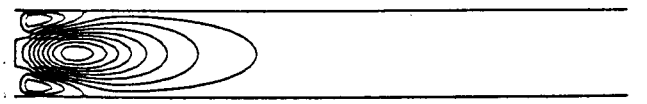

(D) H_y/H_0

Figure 10. Solutions of three-dimensional Hartman flow ($\frac{z}{a} = 0.5$)

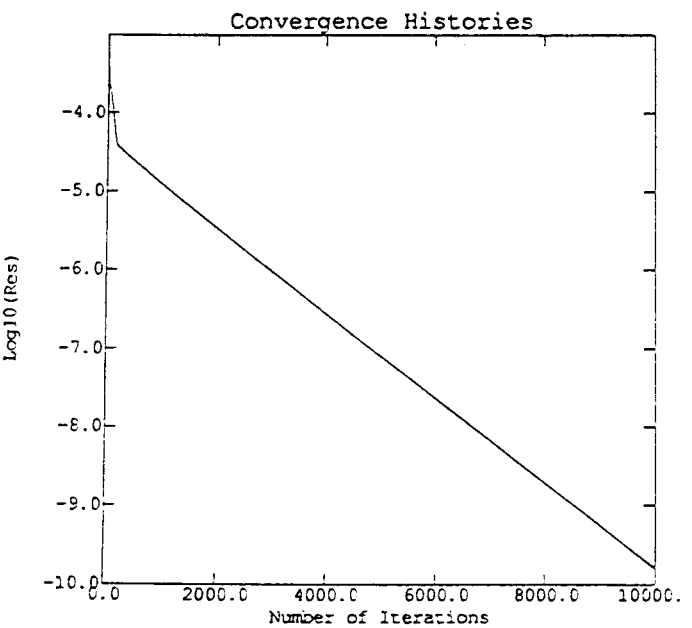

Figure 11. Convergence history (two-dimensional Hartman flow)

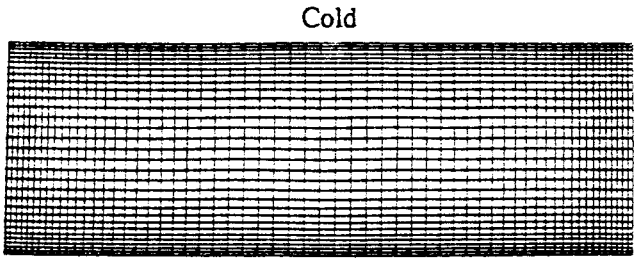

Figure 12. Computational grid of 60×30 cells

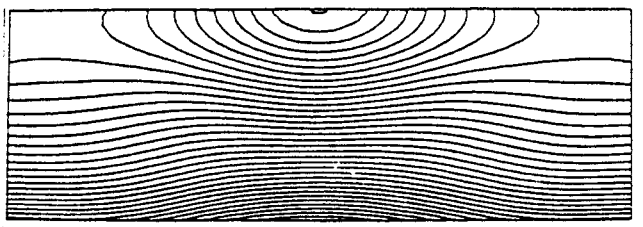

Isobars (without magnetic field)

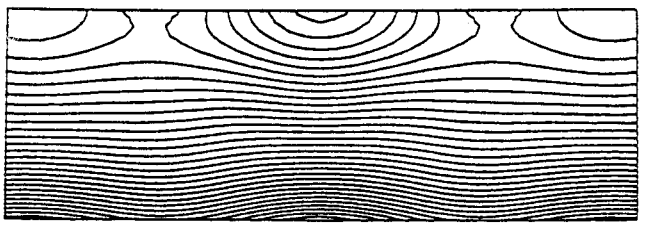

Isobars (with magnetic field)

Figure 13. Isobar contours

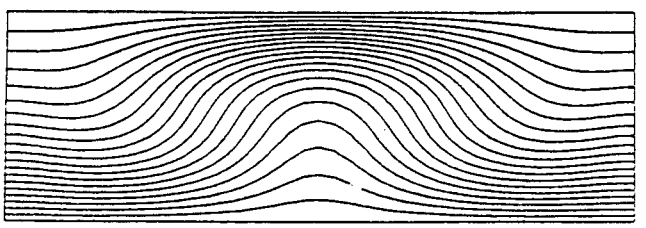

Isotherms (without magnetic field)

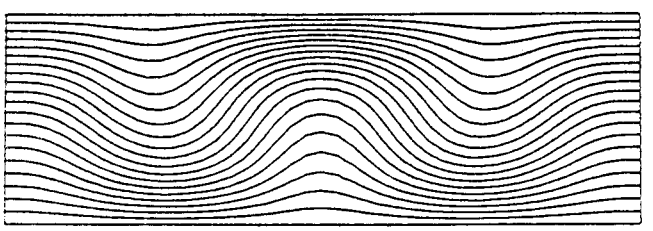

Isotherms (with magnetic field)

Figure 14. Isothermal contours

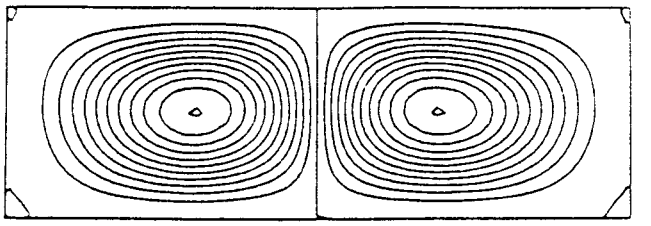

Streamlines (without magnetic field)

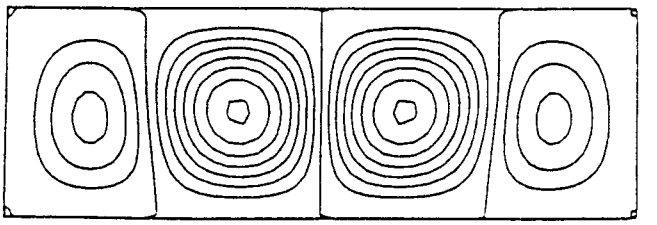

Streamlines (with magnetic field)

Figure 15. Streamlines

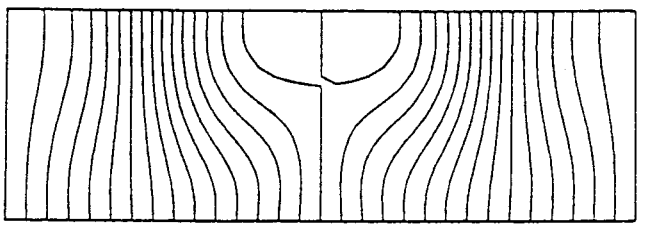

Figure 16. Lines of forces

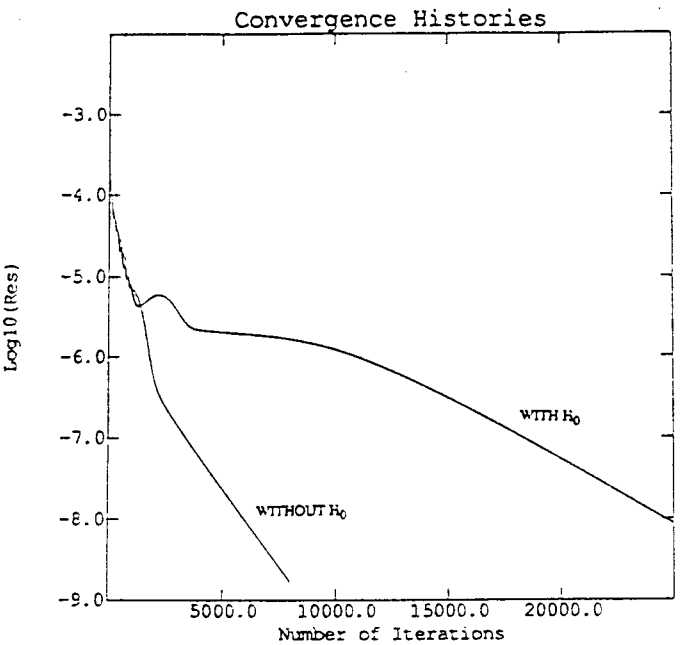

Figure 17. Convergence histories

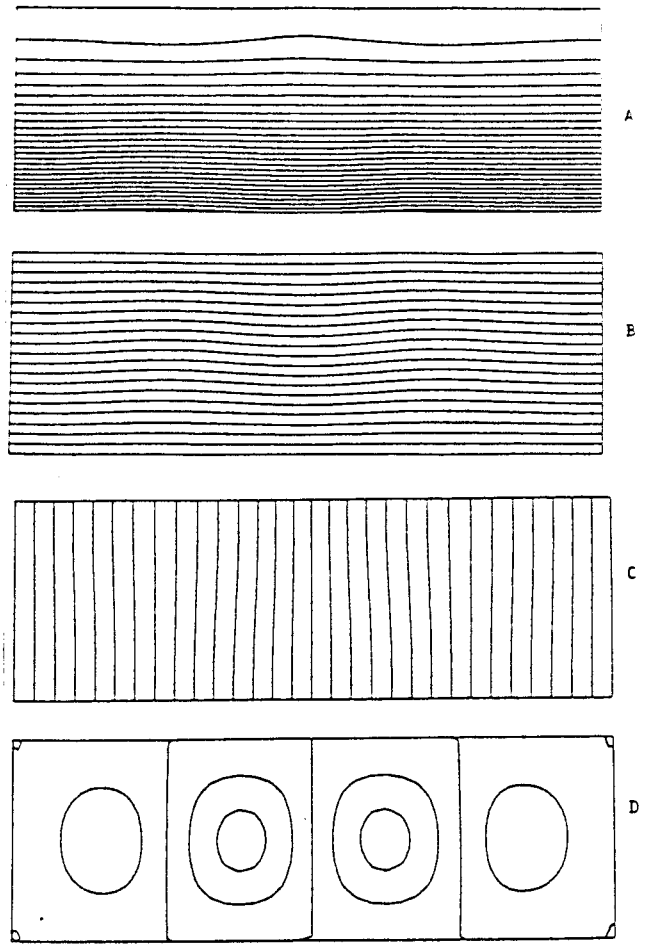

Figure 18. Interaction of a thermally induced flow and a strong magnetic field (Hartman number Ht = 10):
A) isobars; B) isotherms; C) magnetic force lines; D) streamlines